

Quasilocalized charge approximation approach for the nonlinear structures in strongly coupled Yukawa systems

Prince Kumar^{1,2,*} and Devendra Sharma^{1,2,†}

¹*Institute for Plasma Research, Bhat, Gandhinagar, India, 382428*

²*Homi Bhabha National Institute, Training School Complex, Anushaktinagar, Mumbai 400094, India*

(Dated: March 6, 2023)

Strongly coupled systems occupying the transitional range between the Wigner crystal and fluid phases are most dynamic constituents of the nature. Highly localized but strongly interacting elements in this phase possess enough thermal energy to trigger the transition between a variety of short to long range order phases. Nonlinear excitations are often the carriers of proliferating structural modifications in the strongly coupled Yukawa systems. Well represented by a laboratory dusty plasma, these systems show explicit propagation of nonlinear shocks and solitary structures both in experiments and in first principle simulations. The shorter scale length contributions remain absent at strong screening in present approximate models which nevertheless prescribe nonlinear solitary solutions that consequently lose their coherence in a numerical evolution of the system under a special implementation of the quasi-localized charge approximation formulation. The stable coherent structures self-consistently emerge following an initial transient in the numerical evolution which adapts QLCA approach to spatiotemporal domain for accessing the nonlinear excitations in the strong screening limit. The present $\kappa \sim 1$ limit of the existing Yukawa fluid models to show agreement with the experiment and MD simulations has therefore been overcome and the coherent nonlinear excitations have become characterizable up to $\kappa \sim 2.7$, before they become computationally challenging in present implementation.

I. INTRODUCTION

Physical systems exhibiting a strongly coupled phase in the limit of potential energy of interaction exceeding the kinetic or random energy of particles are very effectively modelled by a highly charged minority dust species immersed in an electron-ion plasma. The deterministic configurational correlation between these highly charged species often dominates their response over the kinetic randomness. This most accessible example of a strongly coupled system allows quantitative description of the possible solid and gaseous phases by only two parameters, namely, the coupling parameter $\Gamma = Z^2 e^2 / a k_B T$ and the screening parameter $\kappa = a / \lambda_D$, where λ_D is the plasma Debye length, a is inter-dust separation (Wigner-Seitz radius), Z is dust charge multiplicity of the electronic charge e , T is dust kinetic temperature and k_B is the Boltzmann constant. A vast range of strongly coupled systems modeled by this include dense astrophysical systems [1], warm dense matter, trapped ions [2], ultra-cold neutral plasma [3], etc.

An intermediate state between the so called Wigner crystal [4] ($\Gamma > \Gamma_{\text{melting}}$) phase and the gaseous phase ($\Gamma \sim 0$) remains the most challenging one. This is evident from the fact that a dynamic mean-free version of the random phase (gaseous) approximation [5–8], as well as a solid phase approach acknowledging particle correlation function $g(r)$ [9, 10] have been applied to this intermediate phase with limited success. In accounting for $g(r)$, a

considerable localized stay of dust particles in their fragile (piecewise stable) macroscopic potential landscape is acknowledged just below Γ_{melting} closely resembling the phonon formulation applicable well above Γ_{melting} . This Quasi-localized Charge Approximation (QLCA) is thus applied with a considerable success not only in linear perturbative limit [9, 11] but finite prospects are also explored of its non-perturbative [12] applicability to the nonlinear excitations [13].

In a laboratory setup, dusty plasmas exhibit both molten and crystalline phases of a strongly coupled system [14]. The linear excitations of the dust, namely the the longitudinal dust acoustic waves, and transverse shear modes are well explored by various theoretical models, such as the Generalized Hydrodynamics (GH)[7, 8], thermodynamic approach[15], $T^{(\text{eff})}$ model[16] and Quasi-localized Charge Approximation (QLCA) [9, 17, 18]. In the weak screening regime $\kappa (= a / \lambda_D) \leq 1$ (where a being the lattice constant and λ_D being the debye length), the GH approach described not only of the longitudinal modes but also reproduced the gap at long wavelengths, or the k gap [7, 8], of the transverse (shear) acoustic mode dispersion. The excitation in the strong screening limit ($\kappa \gg 1$) accessed by GH model however depart from the MD simulation dispersion [19] as the original One Component Plasma (OCP) version of the GH model requires essential screening specific corrections both in the equation of state and the excess energy $u(\Gamma)$ which enter its phenomenological dispersion relation [7, 8]. On the other hand, linear dispersions in the strong coupling limit are successfully recovered under the QLCA formulation and the resulting dispersion [9, 10, 17] remains in agreement with experiments [20] and MD simulations [10, 17–19]. The QLCA formula-

* prince.kumar@ipr.res.in

† devendra@ipr.res.in

tion, by accounting for a quasi-localized dust structure, omits dust diffusion to work in the infinite relaxation time limit ($\tau_r \rightarrow \infty$) of the phenomenological dispersion $\omega^2 = c^2 k^2 - \tau_r^{-2}$ [21], hence excludes the k -gap of the transverse dispersion and access $k \rightarrow 0$ excitations. The nonlinear longitudinal excitations, which are subject of the present paper, are treated for the first time under QLCA formulation which besides being in agreement with GH solutions in weak screening limit [22, 23], allows access to the presently unexplored strong screening limit of the nonlinear excitations.

Despite its strength in treating the strong screening regime, the application of QLCA formulation to nonlinear excitations is limited by its intrinsically spectral form largely suitable to linear excitations. This barrier is overcome in the present treatment by adopting the recently developed excluded volume approximation [17] and its numerical implementation for evaluating the QLCA dynamical matrix in the spatiotemporal domain for ready applicability to nonlinear perturbations and examining their stability with respect to temporal evolution. We have first shown that an analytical approximation of the QLCA dynamic matrix D_L [9, 24] in terms of excess energy (the OCP implementation), limited to weak screening limit, reproduces results available from the GH prescription. Applying QLCA formulation in its full capacity to the strong screening limit, we subsequently recover a strong departure of the nonlinear excitations from their weak screening counterparts. The nonlinear structures in this limit are shown to be characteristically distinct when compared to the OCP implementation of the formulation when the latter is nevertheless used to produce nonlinear solutions with relatively larger κ . The access to larger frequency, or shorter wavelength limit, where the OCP based descriptions, including the original GH dispersion as well as its QLCA counterpart, show strong limitation is now available by means of the presented excluded volume approximation of the QLCA dynamical matrix. The corresponding QLCA linear dispersion is shown to closely agree with the results of the MD simulation in this regime. In particular, the $\kappa \sim 1$ limit for the existing Yukawa fluid models to show agreement with the experiment and simulations has been overcome by the present QLCA prescription and agreement is now recoverable up to $\kappa \sim 2.7$.

The article is organized as follows. In Sec. II, the linear QLCA formulation is outlined beginning from a more general rotating frame version of it analyzed recently [25]. The nonlinear approach to excitations with localization accounted for by QLCA formulation within the KdV framework as well as in a general pseudospectral numerical framework are presented in Sec. IIB and Se. III, respectively, alongwith a description of isothermal dust compressibility in Sec. IIC. Impact of the localization on linear and nonlinear analytical solutions of the model is analyzed on KdV-prescribed and more general form of coherent perturbations in Sec. III and Sec. IV, respectively. Summary and conclusions are presented in

Sec. VI

II. NONLINEAR QLCA THEORY FOR A STRONGLY COUPLED YUKAWA SYSTEM

The QLCA theory has been successfully applied to study collective excitation of the liquid phase strongly coupled systems in a rotating [25] as well as non-rotating frame [9]. The microscopic equation of motion of the dust particle in a rotating frame, for the component $r_{i\mu}$ aligned to the direction μ ($= x, y$),

$$m_d \frac{\partial^2 r_{i\mu}}{\partial t^2} = \sum_j K_{ij\mu\nu} r_{j\nu} - 2m_d \left[\boldsymbol{\Omega} \times \frac{\partial \mathbf{r}_i}{\partial t} \right]_\mu - m_d [\boldsymbol{\Omega} \times (\boldsymbol{\Omega} \times \mathbf{r}_i)]_\mu - \frac{\partial V}{\partial r_\mu} = 0, \quad (1)$$

where the second and third terms in the right-hand side are the Coriolis force and centrifugal force, respectively. The quantity V is the dust confinement potential whose gradient balances the corresponding component of the centrifugal force in the typical equilibrium condition [25]. This equation can be reduced, in a non-rotating frame ($\boldsymbol{\Omega} \rightarrow 0$), to a form given as [9],

$$m_d \frac{\partial^2 r_{i\mu}}{\partial t^2} = \sum_j K_{ij\mu\nu} r_{j\nu}, \quad (2)$$

where the non-retarded limit of $K_{ij\mu\nu}$ defines the potential energy of the strongly coupled Yukawa fluid. The particles interact with each other through a shielded potential, namely, the Yukawa potential which is provided by the uncorrelated background plasma, given as,

$$\phi(|\mathbf{r}_i - \mathbf{r}_j|) = e^{-\kappa_b |\mathbf{r}_i - \mathbf{r}_j|} \frac{Z^2 e^2}{|\mathbf{r}_i - \mathbf{r}_j|}, \quad (3)$$

where the screening parameter κ_b is defined by the uncorrelated background plasma pressure and self consistent electric field $\mathbf{E} = \nabla \phi(|\mathbf{r}_i - \mathbf{r}_j|)$ between the negatively charged dust particles can be derived.

The well known linear QLCA results are recovered from equation for the linear perturbation eigenmodes $\xi_{\mathbf{k}\nu}(\omega)$ of $r_{i\mu}$ and an ensemble averaging of the collective coordinates [9, 11],

$$[\omega^2 \delta_{\mu\nu} - C_{\mu\nu}(\mathbf{k}, \omega)] \xi_{\mathbf{k}\nu}(\omega) = 0,$$

where $C_{\mu\nu}$ contains the mean field and local field effects, produced by the random motion and the dust-dust correlation, respectively,

$$C_{\mu\nu}(\mathbf{k}, \omega) = \omega_{pd}^2 \left[\frac{k_\mu k_\nu}{k^2 + \kappa_b^2} + \mathcal{D}_{\mu\nu}(\mathbf{k}, \omega) \right], \quad (4)$$

with ω_{pd} being the dust acoustic frequency. The central quantity in the QLCA, the dynamical matrix in three dimensions, given as,

$$D_{L,T}(\mathbf{k}) = \omega_{pd}^2 \int_0^\infty dr \frac{e^{-\kappa r}}{r} [g(r) - 1] \mathcal{K}_{L,T}(kr, \kappa r), \quad (5)$$

includes dust-dust correlation effects, as this is a functional of the equilibrium pair correlation function (PCF). Clearly, in the absence of any correlations $g(r) \rightarrow 1$ at all values of r , the linear QLCA approach begins to provide the mean-field, or random-phase approximation results ($\mathcal{D}_{\mu\nu} = 0$). Since the desired strong coupling effect enters the formulation predominantly by means of the functional $D_{L,T}$, the nonlinear treatment presented here exploits its adaptation to the spatiotemporal domain while retaining the contributions from the coupling of the individual modes, exclusively achievable under a nonlinear pseudospectral framework[26].

A. Strong coupling in explicit QLCA approach

There remain two options for including the strong coupling effects applicable to two different states of the dust medium, namely, the strong coupling without localization ($g(r) = 1$) and the stronger coupling with finite localization ($g(r) \neq 1$). While the first is achievable by an ad hoc inclusion of strong coupling effects in the pure fluid approach without invoking the QLCA framework since there is no localization, however the second essentially requires QLCA framework as $g(r) \neq 1$ and it is impossible to reduce QLCA to the fluid theory for finite localization limit without reasonable approximations. This puts a natural limit on applicability of the first kind of approach to strongly coupled systems, since when coupling is sufficiently strong finite localization must emerge and the second kind of approach begins to be applicable [11, 27]. We have summarized the (linear) dispersions from treatments belonging to the first option in Appendix VII their relation will be discussed with the nonlinear results obtained by us using the explicit QLCA approach ($g(r) \neq 1$) which show distinction with the existing nonlinear results.

In the limit where D_L is a function of excluded volume parameter $R(\Gamma, \kappa)$ [17], it is derived by choosing a simple but reasonable valid approximation on $g(r)$, i.e., $g(r) = 1$ for $r > R$ and $g(r) = 0$ otherwise, or in a long-wavelength limit, as,

$$D_L = -\omega_0^2(k) + \omega_{pd}^2 e^{-kR} \left[(1 + kR) \left(\frac{1}{3} - \frac{2 \cos kR}{k^2 R^2} + \frac{2 \sin kR}{k^3 R^3} \right) - \frac{\kappa^2}{\kappa^2 + k^2} \left(\cos kR + \frac{\kappa}{k} \sin kR \right) \right] \quad (6)$$

The effective parameter for the excluded volume, $R(\Gamma, \kappa)$, is function of the system state variables, κ and Γ , evaluated using the expression of a system correlation energy. A simple explicit expression for this excluded volume parameter, $R \approx 1 + \frac{\kappa}{10}$, has been calculated for a weak screening regime [28]. In Fig. 1 we have compared the strong-coupling limit linear QLCA dispersion, Eq. (4), with the dispersion in Eq. (A.4), Eq. (A.5) and GH model [8] which admit the strong coupling effects us-

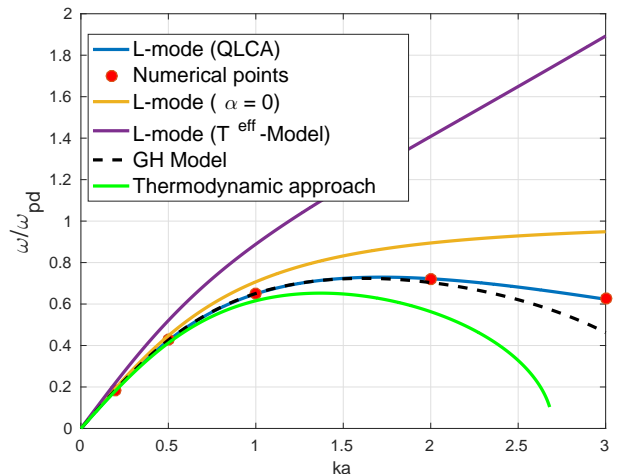


FIG. 1. Analytical (blue lines) and numerical (red dot points) longitudinal wave dispersion relation for the charged dust fluid with values $\Gamma = 185$, $\kappa = 1.0$, and excluded volume $R(\kappa) = 1.1$. The dispersion relation represented by the yellow and purple lines are obtained from a weakly coupled limit ($D_L = 0$) and from a $T^{(\text{eff})}$ model, respectively. The green curve and dash line correspond to the dispersion relation calculated using the thermodynamic approach and GH model, respectively, for the parameters $\kappa = 1$ and $\Gamma = 207$.

ing $T^{(\text{eff})}$, thermodynamic functions and viscoelastic coefficients, respectively, but no explicit localization. The QLCA dispersion relation in Eq. (4) as computed under excluded volume approximation for the case using $\Gamma \approx 180$, $\kappa = 1$ and $R = 1.1$ as in Ref. [17] is plotted in Fig. 1 using blue line which is in agreement with Ref. [17]. The red dots superimposed on the plot are numerically computed dispersion relation by solving, using pseudo-spectral method, the full nonlinear set of QLCA equations under the same approximation showing excellent agreement with linear model at small amplitudes. While the yellow curve saturating to dust acoustic frequency ω_{pd} represents the pure random-phase (fluid-limit) dispersion relation, a contrasting behavior with respect to QLCA dispersion is shown by the dispersion plotted with purple line which is the strong coupling dispersion (A.4) not admitting localization. While the green curve, obtained from the Eq.(A.5) shows correspondence with the QLCA model (blue curve/red dots) at very long wavelength regime ($ka < 1.0$), it shows continuous deviation from the QLCA dispersion at relatively higher mode number ($k \geq 1.0$), as can be seen from the Fig. 1. Note that both the analytical dispersion and the numerical solutions (red dots) obtained from full nonlinear QLCA model implemented by us (red dots in Fig. 1) show agreement also with the Molecular Dynamical(MD) simulations [10, 17] as well as the experimental studies [29]. While the GH model provides good agreement with the QLCA based model at long wavelengths and weak screening limit, it requires presently unavailable corrections for agreement with shorter wavelength and strong screening limit of the dispersion relation recovered in MD simula-

tions [8]. Access to this limit is additionally shown to be possible by a numerical implementation of D_L under the QLCA framework where a more sophisticated form of $g(r)$, derived from MD simulation data, can be used rather than the excluded volume approximation. Results from this implementation are shown to make the comparison with GH model possible up to larger k values in Fig. 2 where

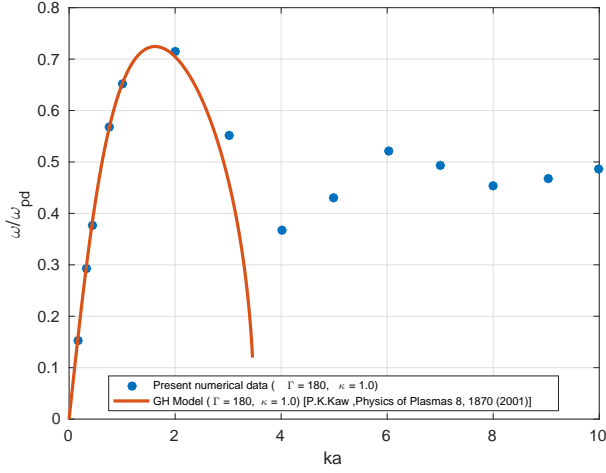


FIG. 2. The red curve corresponds to the dispersion relation obtained from the GH model [8] and the blue dots are plotted using QLCA based model, for same parameter values, $\Gamma = 180$ and $\kappa = 1.0$.

the radial pair correlation function $g(r)$ used in our pseudospectral computations is obtained from the MD simulation data adopted from Ref. [17]. This yields the expression for D_L -matrix,

$$D_L(k) = \omega_{pd}^2 [(-0.568 + 0.3149 \cos(0.431k) + 0.056 \sin(0.431k) + 0.187 \cos(0.862k) + 0.058 \sin(0.862k) + 0.0511 \cos(1.293k) + 0.044 \sin(1.293k) - 0.00016 \cos(1.724k) - 0.025 \sin(1.72k) + 0.0079 \cos(2.155k) - 0.0090 \sin(2.155k))] \quad (7)$$

which is also plotted in Fig. 3 with state parameters $\Gamma = 180$ and $\kappa = 1.0$.

While, as shown in Fig. 2, the GH Model and QLCA predict an identical dispersion relation in a long-wavelength ($ka \leq 2$) limit, in a relatively short wavelength limit the present QLCA based numerical simulations successfully reproduce the oscillatory behavior which is characteristically observed in various theoretical studies [10, 17], MD simulations [30] and experiments [20, 31]. It is therefore clear that the result from the presently available OCP version of the GH model are not a reliable predictor for the short wavelength (high k) excitations. The corresponding $D_L(k)$ plotted in Fig. 3 shows that in the long wavelength regime (small k) the $D_L(k)$ has a variation which corresponds to the $g(r > R) \simeq 1$ as approximated by the excluded volume prescription

[17]. Under this approximation the large r contribution to the wave dynamics dominates over the local interactions. At sufficiently shorter wavelengths (large ka), the strength of $|D_L|$ increases considerably, meaning that the structural effect contribution (i.e., $g(r)$ featuring multiple peaks in Ref. [17]) to the wave dynamics increase significantly, an effect uniquely accounted for by the QLCA formulation.

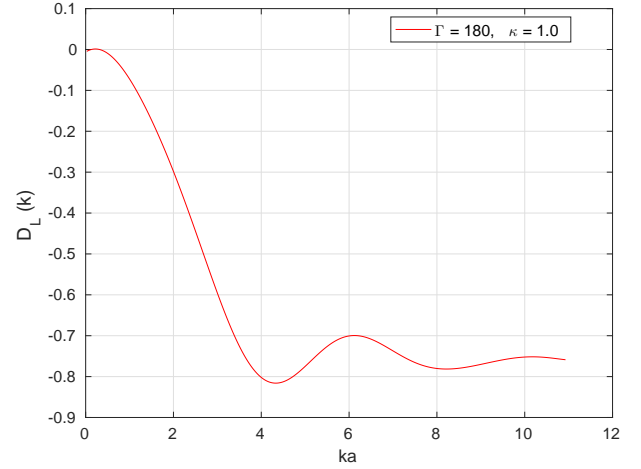


FIG. 3. The plot of D_L -matrix using equation (7) which is obtained from the MD data and dispersion relation given in [17] with $\kappa = 1$.

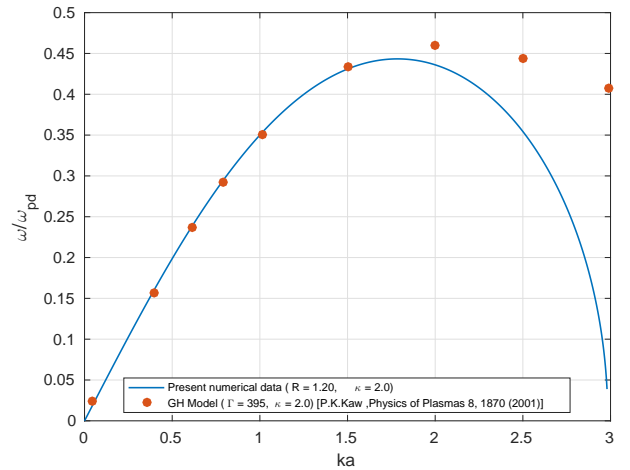


FIG. 4. The blue curve corresponds to the dispersion relation obtained from the GH model [8], $\Gamma = 395$ and $\kappa = 2.0$ and the blue dots are plotted using QLCA based model equation (4) for value, $R=1.20$ and $\kappa = 2.0$.

For the shorter wavelength excitations, however, the discrepancy between the QLCA simulation based predictions (blue dots) and those of the GH model (solid curve) becomes significant. Remarkably, the excluded volume approximation, which uses a simplified step function like profile for the $g(r)$, still produces reasonably good correc-

tion to the linear dispersion, as in Fig. 1, and prescribes frequency values that recover from their steep drop at larger k , to instead saturate to the Einstein frequency [10, 32]. This also remains the reason for a relatively better agreement between even approximate linear QLCA results and the MD simulation data. The comparison between the dispersions from GH and QLCA (excluded volume) for an additional case with higher screening parameter $\kappa = 2.0$ is done in Fig. 4. In both cases the QLCA results remain in agreement also with MD simulations [19] (not reproduced here) up to $ka \sim 3$.

B. Nonlinear excitations of a strongly coupled localized phase dusty plasma

The central idea of localization involves the macroscopic variables obtained from the ensemble averaged particle equations. For a nonlinear approach it is however required that the averages are done over spatiotemporal functions rather than their Fourier transformations. We therefore let the fluid conservation equations represent the evolution of these ensemble averages. We however acknowledge the presence of a spatial ordering of the dust sites by allowing the dynamical matrix $D_{L,T}$ (determining mechanical response of the system) to be computed via the grain-grain correlation energy which changes based on the strain in spatial ordering, in addition to the routine (random phase) response arising from the associated background plasma compression.

This ensemble averaged (macroscopic) momentum equation has same form as Eq. (A.1),

$$\frac{\partial u_{dx}}{\partial t} + (\mathbf{u}_d \cdot \nabla) u_{dx} = \frac{q_d}{m_d} E_x - \frac{1}{m_d n_d} \frac{\partial P_{di}}{\partial x}, \quad (8)$$

where the dust kinetic energy is neglected because of being a few orders smaller than the representative strong coupling term $\frac{\partial P_{di}}{\partial x}$. Similarly, the macroscopic particle continuity equation obtained by ensemble averaging over the dust sites is,

$$\frac{\partial n_{dx}}{\partial t} + \frac{\partial}{\partial x}(n_{dx} u_{dx}) = 0. \quad (9)$$

Separate from the electric field E_x produced by plasma species, the second term in the RHS of Eq. (8) accounts for the electrostatic field produced by the collective shift of the dust particles from their localized positions which must be predominantly restored by the dust structure, rather than purely by E_x . The term is therefore representable as a product of the density gradient produced and a force per unit density gradient. The latter is a rather sophisticated, localization-based, isothermal dust compressibility, treated further, both analytically and numerically, in Sec. II C. It can be noted that, by construction, this new contribution must vanish if (i) there is no structured background dust distribution (i.e., if $g(r) \rightarrow 1$) and/or (ii) if there is no dust density perturbation with respect to this uniform structured dust

background (i.e., if $\partial n_d / \partial x = 0$). The Eq. (8) can therefore be written as,

$$\frac{\partial u_{dx}}{\partial t} + u_{dx} \frac{\partial u_{dx}}{\partial x} = -\frac{q_d}{m_d} \frac{\partial \phi}{\partial x} - \alpha \frac{1}{n_d} \frac{\partial n_d}{\partial x}. \quad (10)$$

where $\alpha_c = \frac{1}{m_d} \frac{\partial P_{di}}{\partial n_d}$ is the isothermal compressibility of the dust. Up on normalization, Eq. (10) takes the form,

$$\frac{\partial u_{dx}}{\partial t} + u_{dx} \frac{\partial u_{dx}}{\partial x} = \mu \frac{\partial \phi}{\partial x} - \tilde{\alpha} \frac{1}{n_d} \frac{\partial n_d}{\partial x}, \quad (11)$$

and the normalized Poisson equation becomes,

$$\frac{\partial^2 \phi}{\partial x^2} = \frac{1}{\mu} [n_d + n_e - n_i], \quad (12)$$

are now taken to be normalized. where we have $\mu = \frac{Z_d T_i}{m_d a^2 \omega_{pd}^2}$, $\tilde{\alpha} = \alpha / \omega_{pd}^2 a^2$, $\delta_e = n_{e0} / Z_d n_{d0}$, $\delta_i = n_{i0} / Z_d n_{d0}$, $n_e = \delta_e (\sigma_i \phi)$, $n_i = \delta_i (-\phi)$ and $\sigma_i = T_i / T_e$, while the equilibrium dust density n_{d0} , the ratio T_i / e , inverse dust acoustic frequency ω_{pd}^{-1} , and mean dust separation a are used as normalizations for the density, potential, time and length, respectively. Eq. (11)-(12) along with the continuity Eq. (9) constitute a nonlinear model. Subject to an accurate representation of α in terms of D_L , this can either be solved numerically, as done by means of the pseudospectral simulation procedure in the present work, or in a rather approximate (and routine) analytical procedure of the reductive perturbation theory [33] (duly done in Sec. II B 1, obtaining the associated KdV equation and its solutions).

The methodology followed here is to first obtain the solutions of the nonlinear KdV equation and use them as initial profiles in our spatiotemporal pseudospectral numerical evolution which covers additional, previously uncovered, parameter regime. More general initial profiles are numerically evolved after this analysis.

1. Derivation of the KdV equation for a strongly coupled fluid

In order to obtain the KdV equation [33] for this system, we first introduce slow variable ζ and τ , given by,

$$\zeta = \epsilon^{1/2}(x - v_0 t), \quad \tau = \epsilon^{3/2} t, \quad (13)$$

where ϵ is a smallness parameter measuring the weakness of the perturbation and V_0 represent the phase velocity of the DAW. In terms of ζ and τ the equations become,

$$\epsilon^{3/2} \frac{\partial n_d}{\partial \tau} - V_0 \epsilon^{1/2} \frac{\partial n_d}{\partial \zeta} + \epsilon^{1/2} \frac{\partial n_d u_d}{\partial \zeta} = 0, \quad (14)$$

$$\epsilon^{3/2} \frac{\partial u_d}{\partial \tau} - V_0 \epsilon^{1/2} \frac{\partial u_d}{\partial \zeta} + \epsilon^{1/2} u_d \frac{\partial u_d}{\partial \zeta} = \mu \epsilon^{1/2} \frac{\partial \phi}{\partial \zeta} - \frac{\alpha}{n_d} \frac{\partial n_d}{\partial \zeta}, \quad (15)$$

and

$$\epsilon^{3/2} \frac{\partial^2 \phi}{\partial \zeta^2} = \frac{1}{\mu} \left\{ \delta_e \left[1 + \sigma_i \phi + \frac{1}{2} \sigma_i^2 \phi^2 + \dots \right] - \delta_i \left[1 - \phi + \frac{1}{2} \phi^2 + \dots \right] + n_d \right\}. \quad (16)$$

We can now expand the variables n_d , u_d and ϕ in the power series of ϵ ,

$$\begin{aligned} n_d &= 1 + \epsilon n_d^{(1)} + \epsilon^2 n_d^{(2)} + \dots \\ u_d &= \epsilon u_d^{(1)} + \epsilon^2 u_d^{(2)} + \dots \\ \phi &= \epsilon \phi^{(1)} + \epsilon^2 \phi^{(2)} + \dots \end{aligned} \quad (17)$$

Substituting Eq. (17) into the Eq. (15), (14) and (16), and equating coefficients of $\epsilon^{3/2}$, we get, to lowest order

$$-V_0 \frac{\partial n_d^{(1)}}{\partial \zeta} + \frac{\partial u_d^{(1)}}{\partial \zeta} = 0, \quad (18)$$

$$-V_0 \frac{\partial u_d^{(1)}}{\partial \zeta} + \alpha \frac{\partial n_d^{(1)}}{\partial \zeta} - \mu \frac{\partial \phi^{(1)}}{\partial \zeta} = 0, \quad (19)$$

and

$$-\frac{h_1}{\mu} \phi - \frac{1}{\mu} n_d^{(1)} = 0, \quad (20)$$

where $h_1 = (\sigma_i \delta_e + \delta_i)$ and $\kappa^2 = \frac{h_1}{\mu} = \frac{a^2}{\lambda_D^2}$. Consequently the Eq. (20) becomes,

$$-\kappa^2 \phi - \frac{1}{\mu} n_d^{(1)} = 0, \quad (21)$$

After integrating and re-arranging terms, the following linear expressions are obtained,

$$u_d^{(1)} = -\frac{\mu V_0}{(V_0^2 - \alpha)} \phi^{(1)}, \quad (22)$$

$$n_d^{(1)} = -\frac{\mu}{(V_0^2 - \alpha)} \phi^{(1)}, \quad (23)$$

and

$$V_0 = \left(\frac{\mu}{h_1} + \alpha \right)^{1/2}. \quad (24)$$

Eq. (24) represents the phase velocity of the dust acoustic wave as a function of α .

Similarly, equating coefficients of $\epsilon^{5/2}$ from Eq. (15), (14) and that of ϵ^2 from Eq. (16), the following equations are obtained,

$$\frac{\partial n_d^{(1)}}{\partial \tau} - V_0 \frac{\partial n_d^{(2)}}{\partial \zeta} + \frac{\partial u_d^{(2)}}{\partial \zeta} + \frac{\partial u_d^{(1)} n_d^{(1)}}{\partial \zeta} = 0, \quad (25)$$

$$\begin{aligned} \frac{\partial u_d^{(1)}}{\partial \tau} - V_0 \frac{\partial u_d^{(2)}}{\partial \zeta} + \alpha \frac{\partial n_d^{(2)}}{\partial \zeta} - \alpha n_d^{(1)} \frac{\partial n_d^{(1)}}{\partial \zeta} \\ + u_d^{(1)} \frac{\partial u_d^{(1)}}{\partial \zeta} - \frac{\partial \phi^{(2)}}{\partial \zeta} = 0, \end{aligned} \quad (26)$$

and

$$\frac{\partial^2 \phi}{\partial \zeta^2} - \left(\frac{h_1}{\mu} \right) \phi^{(2)} + \left(\frac{h_2}{2\mu} \right) (\phi^{(1)})^2 - \frac{1}{\mu} n_d^{(2)} = 0, \quad (27)$$

where $h_2 = (\delta_i - \delta_e \sigma_i^2)$. Eliminating $u_d^{(2)}$, $n_d^{(2)}$ and $\phi^{(2)}$ from Eq. (25)-(27) and making use of Eq. (22)-(24), we find that $\phi^{(1)}$ satisfies the well known KdV equation,

$$\frac{\partial \phi^{(1)}}{\partial \tau} + A \phi^{(1)} \frac{\partial \phi^{(1)}}{\partial \zeta} + B \frac{\partial^3 \phi^{(1)}}{\partial \zeta^3} = 0, \quad (28)$$

where the nonlinear coefficient A and the dispersion coefficient B are given by,

$$A = \left[\frac{\mu \alpha}{2V_0(V_0^2 - \alpha)} - \frac{3\mu V_0}{2(V_0^2 - \alpha)} + \frac{(V_0^2 - \alpha)h_2}{2V_0 h_1} \right] \quad (29)$$

$$B = \frac{(V_0^2 - \alpha)\mu}{2V_0 h_1} \quad (30)$$

with $h_1 = (\sigma_i \delta_e + \delta_i)$ and $h_2 = (\delta_i - \sigma_i^2 \delta_e)$.

Eq. (28) can be solved by separation of variables, giving a solution in the laboratory frame as,

$$\phi(x, t) = \phi_m \operatorname{sech}^2 \left[\frac{\eta}{\Delta} \right], \quad (31)$$

where

$$\phi_m = \frac{3U_0}{A} \quad \text{and} \quad \Delta = \sqrt{\frac{4B}{U_0}}, \quad (32)$$

are the amplitude and width of the soliton, respectively, η is a coordinate in the laboratory frame, and U_0 is the normalized velocity of the solitary wave. In the limit of $\alpha = 0$, these coefficients reduce to well know results, $A = \frac{V_0^3}{2} \left(h_2 - \frac{3}{V_0^4} \right)$, $B = \frac{V_0^3}{2}$, which correspond to the weak coupling limit of the dusty plasma [34].

C. Computation of isothermal dust compressibility from QLCA basics

For treating the general high screening regime of the nonlinear solutions, as central to the present paper, we will be using the more accurate form (6) of the dynamical matrix $D_{L,T}$. However, as presented below, the derivation of $D_{L,T}$ in the analytical form is possible in the weak screening limit to be compared against the nonlinear results from the GH model [22] which uses, and is limited to, the weak screening limit. For this purpose, one might use relationship of α , for example, with the systems correlation energy [5, 6]. In the long-wavelength regime ($ka \leq 2$) as considered in the present case, a model simpler than involving the spectral representations (6) or (7)

of D_L is adopted here for α which essentially reproduces the more general QLCA results presented further below and therefore is equivalent to it [6]. This is realizable because $\alpha = \lim_{k \rightarrow 0} D_L/k^2$ [6, 9] and as long as $g(r)$ does not vary significantly with κ , D_L - matrix remains suitably expressible in term of correlation energy and its derivative, given as [9, 24],

$$D_L(k \rightarrow 0) = \frac{4}{45} \omega_{pd}^2 \left[1 - \kappa \frac{\partial}{\partial \kappa} + \frac{3}{4} \kappa^2 \frac{\partial}{\partial \kappa^2} \right] \frac{E_c(\kappa)}{T_d \Gamma} k^2. \quad (33)$$

Here E_c is the grain-grain correlation energy which can be obtained analytically under the long-wavelength limit [9, 24] for a Yukawa fluid, as,

$$\frac{E_c}{T_d} = a(\kappa)\Gamma + b(\kappa)\Gamma^{1/3} + c(\kappa) + d(\kappa)\Gamma^{-1/3}, \quad (34)$$

where the coefficient up to order κ^4 are given by,

$$a(\kappa) - \frac{\kappa}{2} = -0.899 - 0.103\kappa^2 + 0.003\kappa^4 \\ = a_0 + a_2\kappa^2 + a_4\kappa^4,$$

$$b(\kappa) = 0.565 - 0.026\kappa^2 - 0.003\kappa^4 = b_0 + b_2\kappa^2 + b_4\kappa^4, \\ c(\kappa) = -0.207 - 0.086\kappa^2 + 0.018\kappa^4 = c_0 + c_2\kappa^2 + c_4\kappa^4, \\ d(\kappa) = -0.031 - 0.042\kappa^2 - 0.008\kappa^4 = d_0 + d_2\kappa^2 + d_4\kappa^4, \quad (35)$$

The expression for the α can be obtained by using the value of these coefficients in the equation (34) and then using Eq. (33) [24],

$$\alpha(\kappa, \Gamma) = \lim_{k \rightarrow 0} D_L(k)/k^2 \approx \frac{4}{45\Gamma} \left[\left(a_0 + a_2 \frac{\kappa^2}{2} + 6a_4\kappa^4 \right) \Gamma + \left(b_0 + b_2 \frac{\kappa^2}{2} + 6b_4\kappa^4 \right) \Gamma^{1/3} + \left(c_0 + c_2 \frac{\kappa^2}{2} + 6c_4\kappa^4 \right) + \left(d_0 + d_2 \frac{\kappa^2}{2} + 6d_4\kappa^4 \right) \Gamma^{-1/3} \right].$$

One finds, to leading order in Γ [9],

$$\alpha(\kappa) = -0.0799 - 0.0046\kappa^2 + 0.0016\kappa^4 \quad (36)$$

This dependence of α on parameters Γ and κ defines the effects of dust-dust correlation in a Yukawa system viz. dusty plasma. Since $\alpha(\Gamma, \kappa) < 0$, phase velocity of the dust acoustic wave in a strongly coupled limit given by Eq. (24) is reduced [24] as presented in Fig. 5. The nonlinear effects in the strongly coupled Yukawa system treated here under the QLCA theory can now enter the KdV equation through the coefficients A and B which are also the functions of $\alpha(\Gamma, \kappa)$.

III. NUMERICAL PSEUDO-SPECTRAL COMPUTATION PROCEDURE AND NONLINEAR COHERENT EXCITATIONS

The spatiotemporal domain rather than the spectral (Fourier) domain is adopted for computationally solve

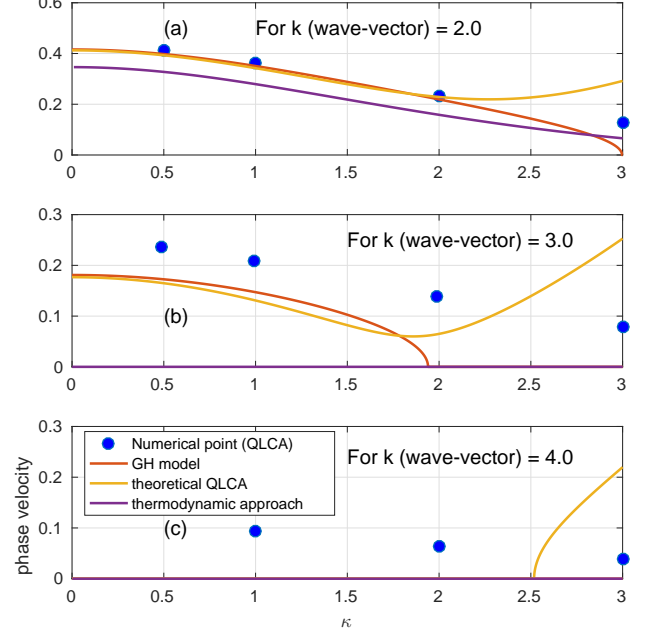


FIG. 5. The variation of the linear phase velocity of the DAW with κ , (a) for fix value of $k = 2.0$, (b) for fix value of $k = 3.0$ and (c) for fix value of $k = 4.0$. The red, yellow and violet curve correspond to the results of the GH model, analytical QLCA based model and thermodynamic approach, respectively. The numerical blue points are plotted using QLCA based model.

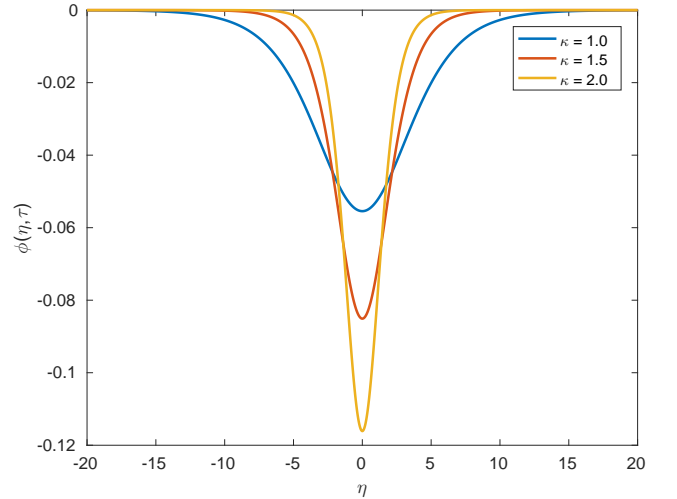


FIG. 6. The variation of the negative solitary potential profile with κ in the analytical QLCA limit (equivalent to GH results), for $h_1 = 4$, $h_2 = 3.9$, $U_0 = 0.1$ and indicated κ values.

the full nonlinear model described by the set of fluid equations (9)-(12), via a full nonlinear pseudo-spectral approach in which the spatial and temporal discretization are possible using the independent variables k and t , respectively, yet, suitably providing the final solutions in the spatiotemporal domain $x-t$. The nonlinear term is calculated by implementing the 2/3-truncate rule in order to avoid the aliasing error [35]. After due verification of the numerical simulation procedure for standard nonlinear problems with known analytic solutions (e.g., in $\alpha = 0$ limit of the model), the localization is included via full spectral version of D_L (6) and (7) to investigate the evolution of the finite amplitude dust acoustic KdV-like solitons.

First, the phase velocity of low amplitude sinusoidal perturbations evolved by the nonlinear pseudo-spectral computations augmented with (6) is compared in Fig. 5 with that obtained from the GH model, thermodynamic approach as well as from the computations where rather approximated (33) model for D_L was used. While the general, full QLCA version of $D_L(k)$ used in numerical pseudospectral simulation (blue points) consistently provides estimates at higher k , the approximate analytical version (33) (effectively underlying both GH and analytical QLCA) shows disagreement and, moreover, missing solutions over increasingly large range of κ values. The red and yellow curves corresponding to phase velocity in GH and analytical QLCA based model, respectively, for the mode $k = 2$ plotted in Fig. 5(a) show agreement with phase velocity in the general numerical model (6) whereas the thermodynamic approach predicts somewhat distinct value for all value of κ . For mode $k = 3$ mode plotted in Fig. 5(b) the phase velocity from GH, analytical QLCA model and thermodynamic approach all begin to show a deviation from the Numerical model (QLCA) results. Moreover, the analytical models do not predict excitable structures beyond $k = 4$ for nearly full range of κ , as presented in Fig. 5(c).

The missing response outlined by Fig. 5 at high k values has finite implications for nonlinear solutions which nevertheless remain obtainable in the form of solutions (31) of the KdV equation [22], despite a bulk of high k constituents not contributing to their construction owing to the limitations of the underlying approximation. Consequently, the evolution of nonlinear structures indeed shows different physical characteristics and considerably sensitivity to κ variation only when obtained by means of the present, more general, numerical QLCA implementation (used for blue dots in Fig. 5) as analyzed below using coherent perturbations.

As presented in Fig. 7, the general present pseudospectral simulations (red) initialized using the solutions (31) of the KdV equation as initial condition (stationary blue profiles) show an initial transient until the solitary structures settle down to newer stably propagating solitary profiles which are distinct from what prescribed by the analytical approximation based high κ QLCA solutions (which agree with GH solutions). These newer coherent

solitary structures are far steeper than those predicted by the analytical approximation underlying the KdV equation. At relatively higher κ values the numerical solution tend to grow extremely steep and acquire cusp-like spatial profiles showing weaker temporal coherence. The accessibility to their evolution with enough accuracy is thus seen to also depend on the numerical resolution of the computations. Remarkably, this initial transient is

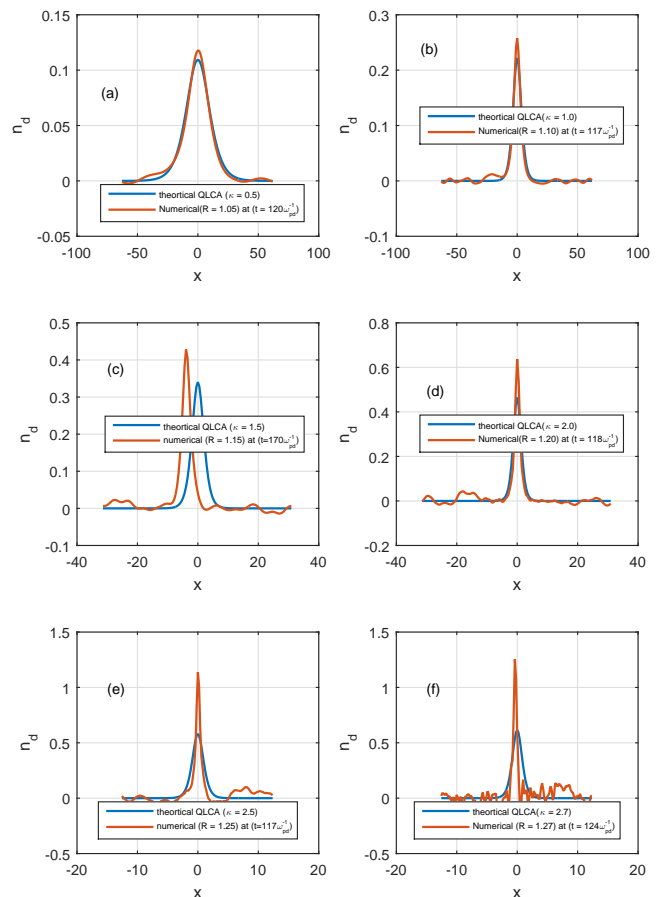


FIG. 7. The solitary density profile with, (a) $\kappa = 0.5$, (b) $\kappa = 1.0$, (c) $\kappa = 1.5$, (d) $\kappa = 2.0$, (e) $\kappa = 2.5$, (f) $\kappa = 2.7$, in both the numerical and analytical limit of the QLCA theory, for $h_1 = 4$, $h_2 = 3.9$, $U_0 = 0.1$

not produced in pseudospectral numerical evolution in the low κ , or weak screening, regime and the initial profiles prescribed by the analytical KdV solutions propagate without any significant distortion, indicating that both analytical QLCA and the GH model make a reasonably good prediction of the nonlinear coherent structures, remaining in agreement with the general numerical implementation. Additionally, the numerical approaches using D_L based on (6) and (7) were also compared and found to be nearly in agreement with each other. The red

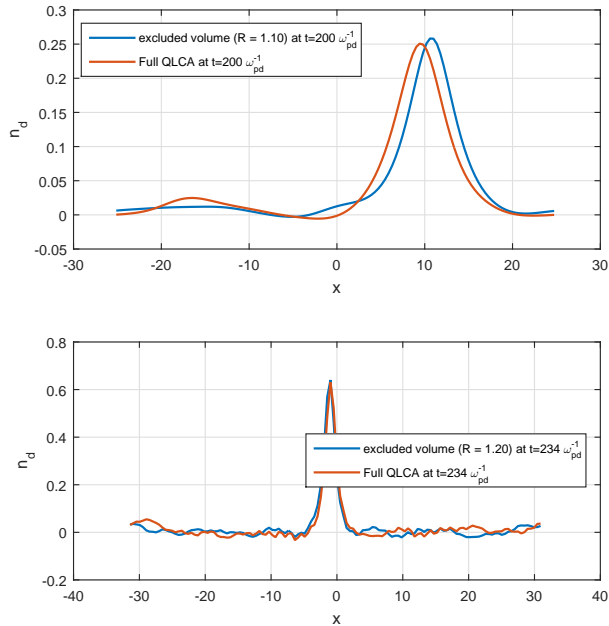


FIG. 8. The solitary density profile with, (a) Excluded volume ($R = 1.10$), (b) Excluded volume $R = 1.20$, in both the Excluded volume approximation and Full QLCA D_L matrix, for $h_1 = 4$, $h_2 = 3.9$, $U_0 = 0.1$.

and blue curve, in Fig. 8 (a), correspond to the soliton structure obtained from the full QLCA D_L matrix with $\kappa = 1.0$ and excluded volume approximation with $R = 1.10$, respectively. There is no significance difference observed to be developed, accordingly, in the soliton structure. Similar behavior of the soliton structures can also be seen from Fig. 8(b) at relative higher screening parameter value $\kappa = 2.0$ in which the soliton structures obtained from both the full QLCA D_L matrix with $\kappa = 2.0$ and Excluded volume approximation with $R = 1.20$, respectively, almost overlap.

The agreement between GH model solutions with the numerical computations in smaller κ regime relates, more quantitatively, to the characteristics of linear modes for lower and higher k values, which is analyzed over a range of κ values, for example in Fig. 5. Only a moderate variation of $g(k)$ with κ for lower k means that $D(k \rightarrow 0)$ can still be derived from the system correlation energy and its derivatives. No analytical approximation is however possible for relatively higher values of k and κ , and D_L remains no longer correctly expressible in terms of the system correlation energy. On the other hand, the general adaptations of D_L , either (6) or (7), by means of our pseudospectral (spatiotemporal, yet fully resolved in the k values of modes constituting the nonlinear structures) numerical model, accounting for the structural effects continues to describe the smaller wavelengths and relative stronger screened excitations in this limit. Therefore, Numerical simulation accounting for the full structural

effects can suitably describe the higher wavelengths and relative stronger screened excitations in such systems.

IV. CHARACTERIZATION OF ANALYTICAL NONLINEAR SOLITARY SOLUTIONS IN WEAK SCREENING LIMIT

In order to analyze solitary waves in a strongly coupled but weakly screened dusty plasma with finite localization in rather detail, we begin by presenting the amplitude ϕ_m and width Δ of the soliton given by Eq. (32) (besides normalized velocity of the U_0). The amplitude ϕ_m and width Δ depend on α and, in turn, on κ and Γ through factors A and B given by Eq. (29) and (30), respectively. The negative solitary potential profile is plotted in Fig. 6 in the strong coupling (QLCA) limit with different values of screening parameter κ . For the constant value of U_0 , the amplitude of the solitary wave increases with κ in

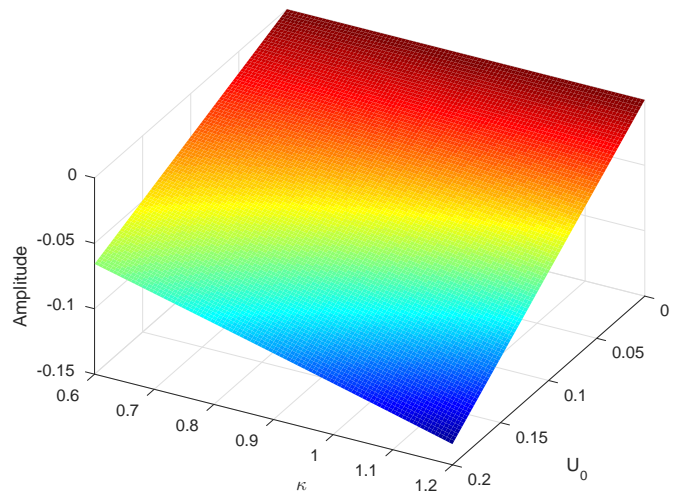


FIG. 9. The variation of the amplitude of the negative solitary potential with parameters κ and U_0 for constant value of $h_1 = 4$, $h_2 = 3.9$.

strongly coupled (QLCA) limit since the amplitude has an inverse dependence on with factor A reduces with κ in this limit. The width being directly proportional to factor B reduces with κ in the strongly coupled (QLCA) limit. This behavior of solitary waves explored for the strongly coupled and localized phase of the dust (adopting QLCA based approach) is in contrast to the effects of strong coupling on a dust solitary wave analyzed in a model where strong-coupling effects are introduced via an effective temperature $T^{(\text{eff})}$ [36]. A better agreement the soliton solutions recovered in the present treatment is however seen with the Molecular Dynamical (MD) simulation results [37, 38]. Moreover, the behavior of solitary waves explored by adopting QLCA based approach is also in contrast to the effects of dust temperature on a

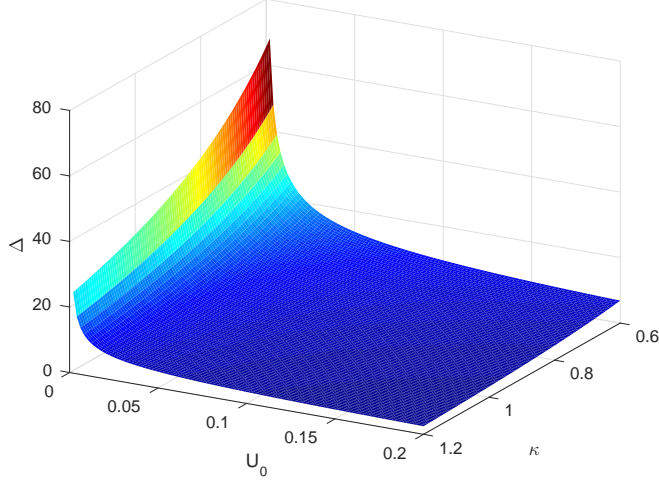


FIG. 10. The variation of the width of the negative solitary potential with parameters κ and U_0 for constant value of $h_1 = 4$, $h_2 = 3.9$.

dust solitary wave analyzed from the theoretical models [39, 40] in which the amplitude and width of dust acoustic solitary waves decreases and increases, respectively, with increasing the dust temperature.

The 2D surface plot of the amplitude ϕ_m and width Δ of the dust solitary waves are presented in Fig. 9 and 10, respectively, describing their variation with respect to variation of the parameters U_0 and α . For a fix value of α , while the amplitude of the dust solitary wave increases with U_0 its width is shown to decrease, which is a behavior consistent with the well known characteristics of the solitons where the product $|\phi_m|\Delta^2$ is independent of U_0 .

V. SIMULATIONS WITH INITIAL PROFILES OF GENERAL FORM

For simulating more general but initially localized non-linear perturbations, we have also launched a more general, Gaussian-shaped, initial density perturbations in the pseudospectral simulation procedure given by,

$$n_d = n_0 \exp \left[- \left(\frac{x - x_0}{\Delta} \right)^2 \right], \quad (37)$$

Fig. 11 presents the evolution of the initial Gaussian density perturbation, with $n_0 = 0.05$, $\Delta = 20$ and $x_0 = 64$, in both strong ($\alpha \neq 0$, $R = 1.1$) and weak ($\alpha = 0$) coupling limit of the model. It is evident from the presented evolution that in the weakly coupled limit the perturbation decays into two unequal solitons, whereas it splits in to three unequal amplitude soliton structures when the dust-dust correlations are accommodated in the model with complete localization effects. It can be seen that

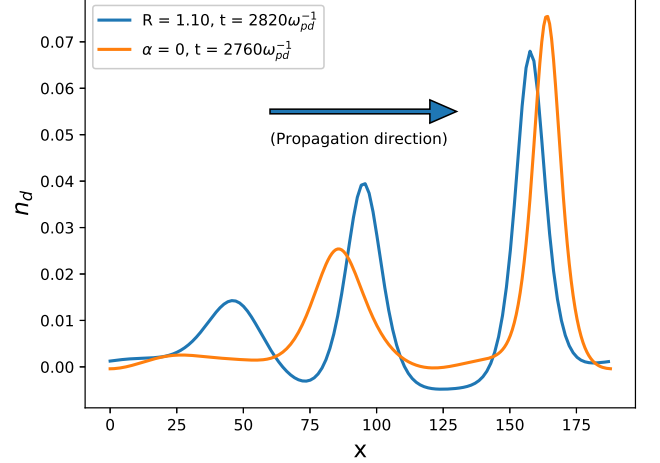


FIG. 11. Time evolution profile of an initial Gaussian dust density perturbation in the both weak and strong coupling limit for $\kappa = 1.0$, $n_0 = 0.05$ and $\Delta = 20$.

the taller soliton propagates with a velocity faster than the smaller soliton which remains a well know property of the soliton/solitary wave structures of KdV type.

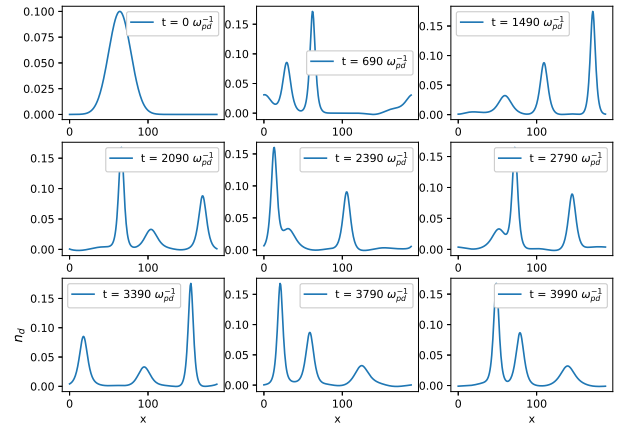


FIG. 12. Time evolution of an initial Gaussian dust density perturbation profile in a weakly coupled limit for $\kappa = 1.0$, $n_0 = 0.1$ and $\Delta = 20$.

A number of more general initial condition structures with a range of initial amplitude are studies further in order to understand the influence, on these excitations, of various initial density perturbation profiles. Fig. 12 presents the evolution of a density perturbation with a relatively higher initial amplitude $n_0 = 0.1$ within the weak-coupling limit ($\alpha = 0$). The emergence of three unequal height soliton has once again been noted in this case which appears identical to the strong-coupling case presented in Fig. 11. It can therefore be concluded that

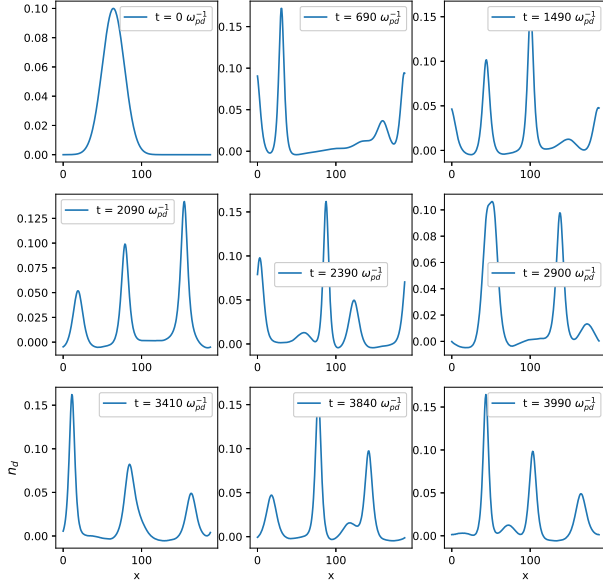


FIG. 13. Time evolution of an initial Gaussian dust density perturbation profile in the strongly coupled limit for $\kappa = 1.0$, $R(\kappa) = 1.10$, $n_0 = 0.1$ and $\Delta = 20$.

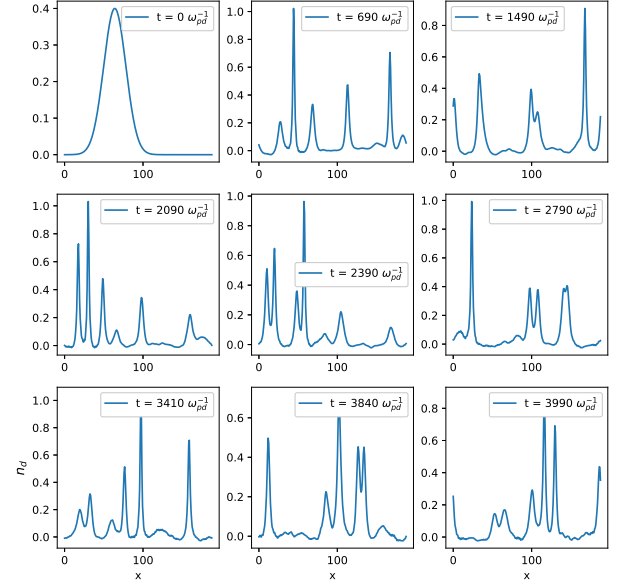


FIG. 15. Time evolution of an initial Gaussian dust density perturbation profile in the strongly coupled limit for $\kappa = 1.0$, $R(\kappa) = 1.10$, $n_0 = 0.4$ and $\Delta = 20$.

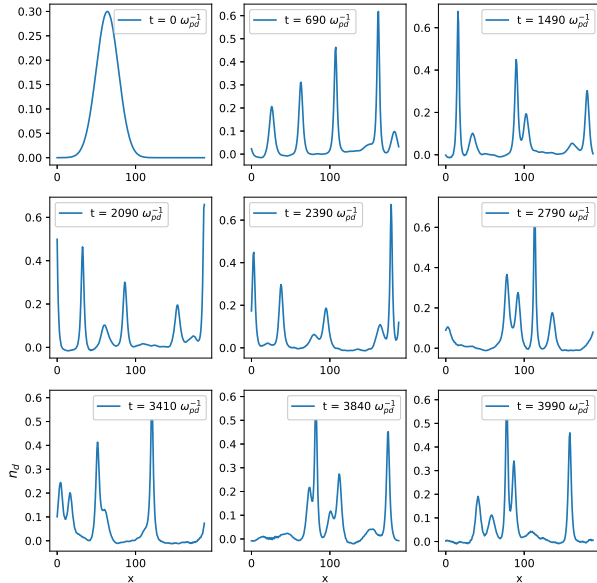


FIG. 14. Time evolution of an initial Gaussian dust density perturbation profile in the strongly coupled limit for $\kappa = 1.0$, $R(\kappa) = 1.10$, $n_0 = 0.3$ and $\Delta = 20$.

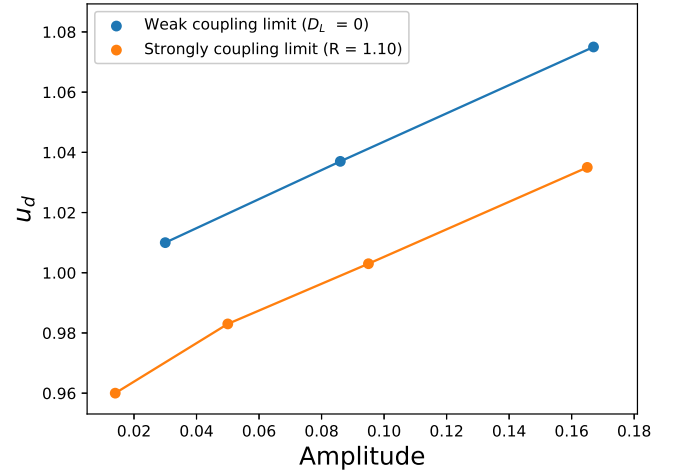


FIG. 16. Mach Number (u_d) of the dust acoustic solitons as a function of their amplitude in the weak and strongly coupling limit for $\kappa = 1.0$ and $n_0 = 0.1$.

the effect of strong-coupling is somewhat equivalent to the choice of an increased initial amplitude of the perturbation. The next Fig. 13 presents the evolution of the density perturbation with the initial amplitude $n_0 = 0.1$ however this time in the strong-coupling limit. What is noted is the emergence of a train of four solitons of orderly reducing heights, confirming the equivalence of

strong-coupling to the initial amplitude of the perturbation. Since these solitary structures visibly preserve their identities for a considerably longer time (i.e., several orders of inverse dust acoustic frequency) and even after undergoing mutual interaction (or collisions), they indeed represent the dust acoustic soliton structures. Fig. 14 and 15 demonstrate the reasonably consistent solitary evolution of the initial density perturbation with even higher amplitudes, $n_0 = 0.3$ and $n_0 = 0.4$, respectively, up to a sufficiently longer evolution time $\omega_{pd}t = 3900$.

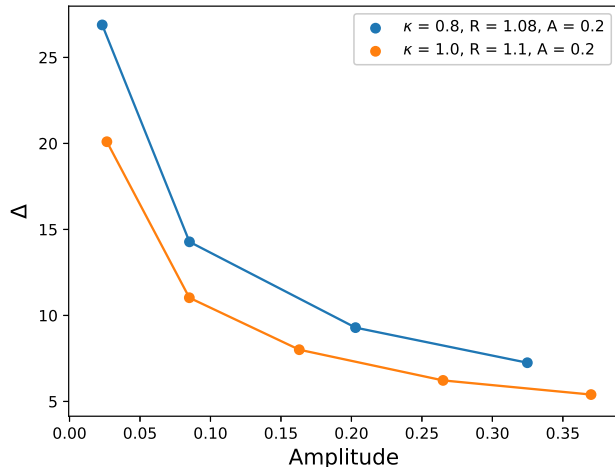


FIG. 17. Width (Δ) of the dust acoustic solitons as a function of their amplitude in the strong coupling limit for different value of parameter $R(\kappa)$.

In order to make a comparison with the theoretical estimates presented in Sec. II, the normalized velocity (to linear dust acoustic velocity) and width of the dust acoustic solitons are presented in Figs. 16 and 17, respectively. These are measured for different excitation amplitudes after the individual solitons appear in both weak and the strong coupling cases. The Mach number u_d of the solitary wave increases linearly with amplitude in both strong and weakly coupled limit consistent with the experimental observations[22, 41, 42]. The measured Mach number u_d of the solitons in the strong-coupling is smaller than in the weak coupling ($\alpha = 0$) limit of the model. The effect of the strong dust-dust correlation in reducing the phase velocity of the solitons, is consistent with the theoretical predictions of Sec. II. For a fixed value of $R(\Gamma, \kappa)$ (the excluded volume parameter) the width of a soliton decreases with increasing the amplitude, as can be seen from Fig. 17. On the other hand, for a fixed value of the soliton amplitude, the width of a soliton decreases with increasing the dust-dust correlation via parameter κ or $R(\Gamma, \kappa)$. This effect of the dust-dust correlation is also in correspondence with the above theoretical prediction of Sec. II. Finally, in order to present a more quantitative aspect of the presented numerical soliton solutions we conclude by presenting another well known property of

Amplitude(A)	Width(Δ)	($A\Delta^2$)
0.0235	26.90	17.040
0.0851	14.28	17.350
0.2029	9.292	17.518
0.3248	7.251	17.077

TABLE I. The soliton characteristic property for the parameters $\kappa = 0.8$, $R(\kappa) = 1.08$ and $A = 0.2$.

the Kdv solitons, namely, the product of amplitude and squared width, $\phi_m \Delta^2$, of the solitons which remains independent to the dust acoustic soliton mach number. Our solutions confirm that this property of the dust acoustic soliton is preserved and persists even in the realm of the QLCA approach applied to the soliton formulation, as presented in the form of data in Table I.

VI. SUMMARY AND CONCLUSIONS

To summarize, the nonlinear approach is made to finite amplitude excitations of strongly-coupled fluids such that dust localization effects are present and can not be neglected especially while treating strong screening of localized charges generated by the background plasma, for example in a laboratory dusty plasma. The nonlinear excitations treated under analytical approximations that exclude localization nevertheless prescribe localized solutions with very limited reproducibility by a numerical implementation of more full nonlinear model accounting for the localization by means of the dynamical matrix D_L under the quasi-localized charge approximation. Inclusion of the finite dust localization, essentially requiring to account for the structured pair-correlation function $g(r)$, is suitably facilitated by the quasi-localized charge approximation framework. With its present applications remaining limited to spectral domain and hence largely to exploring the linear dispersions, the persisting challenge of inclusion of these effects in a full nonlinear and therefore spatiotemporal formulation is addressed in the present study. This is done by developing and solving an analytical nonlinear model for the localized-phase of a strongly coupled dusty plasma system while incorporating the elements of detailed QLCA formulation. The nonlinear solutions are obtained both by analytical and numerical implementations, in a nonlinear pseudospectral approach, of the dynamical matrix D_L duly accounting for a structured pair-correlation function $g(r)$. The characterization of both periodic and coherent solitary nonlinear structures has allowed to identify, in strong screening limit, the contribution over a considerable spectral range spectral which is adequately accounted for by a more general QLCA implementation of the localization by means of nonlinear pseudospectral procedure.

Among main results, we have first shown that an analytical approximation of the QLCA dynamic matrix

D_L [9, 24] in terms of excess energy (the OCP implementation), limited to weak screening limit, reproduces results available from the GH prescription. However, application of the QLCA formulation in its full capacity to the strong screening limit subsequently allows recovery of a strong departure in the evolution of the nonlinear excitations from that of their weak screening counterparts, accessed by OCP limit implementation of the procedure well within QLCA framework. Accordingly, the nonlinear pseudospectral procedure initialized with the analytical coherent solitary solutions of the KdV equation although propagate unmodified in the small κ limit, they undergo an initial transient and self-consistently settle down to newer more steeper profiles for large κ values. At relatively higher κ values the numerical solutions tend to grow extremely steep and acquire cusp-like spatial profiles showing weaker temporal coherence indicating that they are rather governed by a modified KdV equation, as supported by certain recent arguments[43, 44]. The observations that the accessibility to their evolution with enough accuracy is only limited by the numerical resolution of the computations indicate potential applicability of the analysis procedure to rather yet unexplored limits of the parameter space.

In terms of linear structures, the access to larger frequency, or shorter wavelength limit, where the OCP based descriptions, including the original GH dispersion as well as its QLCA counterpart, show strong limitation is now available by means of the presented excluded volume approximation of the QLCA dynamical matrix. The corresponding QLCA linear dispersion is shown to closely agree with the results of the MD simulation in this regime. In essential quantitative terms, the $\kappa \sim 1$ limit for the existing Yukawa fluid models of both periodic linear and coherent nonlinear excitations to show agreement with the experiment and simulations has been overcome by the present QLCA prescription and agreement is now recoverable up to $\kappa \sim 2.7$.

Among its major limitations, the QLCA approach remains unsuitable to an arbitrarily large κ . It also loses its applicability when approaching the hard sphere interaction limit [45]. The nonlinear processes involving unstable density fluctuations of shorter wavelength, for example, DAW suffer a modulational instability at short wavelengths, can however be captured by the QLCA model and a related nonlinear analysis is being communicated by the authors separately, which also forms a suitable future work to the present study.

VII. ACKNOWLEDGMENT

The simulation work presented here is performed on ANTYA cluster at the Institute for Plasma Research (IPR), Gandhinagar, India.

Appendix: Incorporation of the strong coupling effects without localization

1. Effective strong coupling in random phase limit

While explicit representation of strong coupling by retaining the correlation via dynamical matrix $D_{L,T}$ is central to QLCA approach, a strongly coupled yet random phased state ($g(r) \rightarrow 1$) is treatable by an effective representation of the dust-dust correlation by supplementing the kinetic dust pressure, P_{dk} , by an effective pressure, P_{di} , or an isothermal dust compressibility [36],

$$\frac{\partial u_{dx}}{\partial t} + (\mathbf{u}_d \cdot \nabla)u_{dx} = \frac{q_d}{m_d}E_x - \frac{1}{m_d n_d} \left[\frac{\partial P_{dk}}{\partial x} + \frac{\partial P_{di}}{\partial x} \right]_1$$

An effective temperature $T_d^{(\text{eff})}$, apart from dust kinetic temperature is then used to express the compressibility arising from the correlations,

$$\frac{\partial u_{dx}}{\partial t} = \frac{q_d}{m_d}E_x - \frac{T_d^{(\text{eff})}}{m_d n_d} \frac{\partial n_d}{\partial x}, \quad (\text{A.2})$$

where,

$$T_d^{(\text{eff})} = \frac{N_{nn}}{3} \Gamma T_d (1 + \kappa) \exp(-\kappa), \quad (\text{A.3})$$

which is a few orders of magnitude higher than the kinetic temperature of the dust.

Eq. (A.2) along with the continuity and Poisson equations produces the linear dispersion relation of the strongly coupled dusty plasma in the random phase limit,

$$\omega^2 = \left(\frac{d_1 k^2 \omega_{pd}^2}{1 + k^2} \right) + \beta k^2, \quad (\text{A.4})$$

where β and d_1 are the model parameters defined by the dust and background plasma [36].

2. Thermodynamic approach to the strong-coupling in random phase limit

One of the simplest approaches to account for the strong coupling effects in this limit has been presented by Khrapak [15] in which strong coupling effects are included in the conventional fluid model by supplementing it with the appropriate thermodynamic functions,

$$c_s^2 = \frac{\omega^2}{k^2} = \omega_{pd}^2 \left(\frac{1}{\kappa^2} + \frac{\gamma \mu}{3\Gamma} \right), \quad (\text{A.5})$$

where γ and μ is the adiabatic index and isothermal compressibility modulus, respectively. To evaluate the effects of strong coupling on the dispersion relation and sound velocity of Yukawa fluid, the parameter γ and μ

are represented in term of thermodynamic functions of Yukawa fluid as,

$$\gamma\mu = \mu + \frac{[p - \Gamma(\partial p/\partial\Gamma)]^2}{u - \Gamma(\partial p/\partial\Gamma)}, \quad (\text{A.6})$$

where u , p and μ are the internal energy, pressure and isothermal compressibility modulus, respectively, which account for the both particle-particle correlation and plasma-related effects [46]. These linear dispersion are compared with the more general linear dispersion generated by QLCA of linear perturbation equation (4), obtained as below. With the isothermal compressibility having negative sign, at sufficiently strong coupling this results in the loss of solution at large k values, leading to null frequency observed in dispersion relation plotted with a green line in Fig. 1. This issue is effectively resolved by inclusion of localization in QLCA model as

discussed further below.

3. Generalized hydrodynamic model (GH)

The GH model, based on phenomenological dispersion [8], incorporates the strongly coupling effects via nonlocal visco-elasticity with memory effects arising from the strong correlation among constituent particles. In a long wavelength limit, the dispersion relation of strongly coupled yukawa system in their kinetic regime can be written as,

$$\omega^2(k) = \frac{\omega_{pd}^2 k^2}{k^2 + \kappa^2} + \frac{\omega_{pd}^2 k^2}{\Gamma} \left(\frac{1}{3} + \frac{4}{45} u_{ex} \right), \quad (\text{A.7})$$

where u_{ex} is the normalized excess energy given in Ref. [8].

-
- [1] F. Peng, E. F. Brown, and J. W. Truran, *The Astrophysical Journal* **654**, 1022 (2007).
- [2] A. Dantan, J. Marler, M. Albert, D. Guénot, and M. Drewsen, *Physical review letters* **105**, 103001 (2010).
- [3] T. C. Killian, T. Pattard, T. Pohl, and J. Rost, *Physics reports* **449**, 77 (2007).
- [4] X. Wang, A. Bhattacharjee, and S. Hu, *Phys. Rev. Lett.* **86**, 2569 (2001).
- [5] L.-J. Hou, Y.-N. Wang, and Z. Mišković, *Physical Review E* **70**, 056406 (2004).
- [6] L.-J. Hou, Z. Mišković, A. Piel, and M. S. Murillo, *Physical Review E* **79**, 046412 (2009).
- [7] P. Kaw and A. Sen, *Physics of Plasmas* **5**, 3552 (1998).
- [8] P. Kaw, *Physics of Plasmas* **8**, 1870 (2001).
- [9] K. I. Golden and G. J. Kalman, *Physics of Plasmas* **7**, 14 (2000).
- [10] Z. Donko, G. J. Kalman, and P. Hartmann, *Journal of Physics: Condensed Matter* **20**, 413101 (2008).
- [11] G. J. Kalman, K. I. Golden, Z. Donko, and P. Hartmann, *Journal of Physics: Conference Series* **11**, 254 (2005).
- [12] K. I. Golden, G. J. Kalman, Z. Donko, and P. Hartmann, *Journal of Physics A: Mathematical and Theoretical* **42**, 214017 (2009).
- [13] C.-J. Lee and G. J. Kalman, *Journal of the Korean Physical Society* **58**, 448 (2011).
- [14] G. E. Morfill and A. V. Ivlev, *Reviews of modern physics* **81**, 1353 (2009).
- [15] S. A. Khrapak and H. M. Thomas, *Physical Review E* **91**, 033110 (2015).
- [16] V. Yaroshenko, V. Nosenko, and G. Morfill, *Physics of Plasmas* **17**, 103709 (2010).
- [17] S. A. Khrapak, B. Klumov, L. Couedel, and H. M. Thomas, *Physics of Plasmas* **23**, 023702 (2016).
- [18] G. Kalman, M. Rosenberg, and H. DeWitt, *Physical review letters* **84**, 6030 (2000).
- [19] H. Ohta and S. Hamaguchi, *Physical Review Letters* **84**, 6026 (2000).
- [20] S. Nunomura, S. Zhdanov, D. Samsonov, and G. Morfill, *Physical review letters* **94**, 045001 (2005).
- [21] C. Yang, M. Dove, V. Brazhkin, and K. Trachenko, *Physical review letters* **118**, 215502 (2017).
- [22] S. Sharma, A. Boruah, and H. Bailung, *Physical Review E* **89**, 013110 (2014).
- [23] A. Boruah, S. Sharma, Y. Nakamura, and H. Bailung, *Physics of Plasmas* **23**, 093704 (2016).
- [24] M. Rosenberg and G. Kalman, *Physical Review E* **56**, 7166 (1997).
- [25] P. Kumar and D. Sharma, *Physics of Plasmas* **28**, 083704 (2021).
- [26] B. Fornberg, *A practical guide to pseudospectral methods*, 1 (Cambridge university press, 1998).
- [27] Z. Donkó, P. Hartmann, and G. Kalman, *Physics of Plasmas* **10**, 1563 (2003).
- [28] S. A. Khrapak, *AIP Advances* **7**, 125026 (2017).
- [29] P. Bandyopadhyay, G. Prasad, A. Sen, and P. Kaw, *Physics Letters A* **368**, 491 (2007).
- [30] A. V. Mokshin, I. I. Fairushin, and I. M. Tkachenko, *Physical Review E* **105**, 025204 (2022).
- [31] S. Zhdanov, S. Nunomura, D. Samsonov, and G. Morfill, *Physical Review E* **68**, 035401 (2003).
- [32] C.-S. Wong, J. Goree, and Z. Haralson, *IEEE Transactions on Plasma Science* **46**, 763 (2017).
- [33] R. Davidson, *Methods in nonlinear plasma theory* (Elsevier, 2012).
- [34] P. K. Shukla and A. Mamun, *Introduction to dusty plasma physics* (CRC press, 2015).
- [35] E. Coutsias, F. Hansen, T. Huld, G. Knorr, and J.-P. Lynov, *Physica Scripta* **40**, 270 (1989).
- [36] S. E. Couzens, S. Sultana, I. Kourakis, V. V. Yaroshenko, F. Verheest, and M. A. Hellberg, *Physical Review E* **86**, 066404 (2012).
- [37] S. K. Tiwari, A. Das, A. Sen, and P. Kaw, *Physics of Plasmas* **22**, 033706 (2015).
- [38] S. Kumar, S. K. Tiwari, and A. Das, *Physics of Plasmas* **24**, 033711 (2017).
- [39] A. Mamun and P. Shukla, *Physica Scripta* **2002**, 107 (2002).
- [40] A. Mamun and P. Shukla, *Plasma physics and controlled fusion* **47**, A1 (2005).

- [41] V. Nosenko, S. Nunomura, and J. Goree, Physical review letters **88**, 215002 (2002).
- [42] P. Bandyopadhyay, G. Prasad, A. Sen, and P. Kaw, Physical review letters **101**, 065006 (2008).
- [43] J. K. Hunter and R. Saxton, SIAM Journal on Applied Mathematics **51**, 1498 (1991).
- [44] S. Kumar Tiwari, A. Das, P. Kaw, and A. Sen, Physics of Plasmas **19**, 013706 (2012).
- [45] S. Khrapak, B. Klumov, and L. Couëdel, Scientific Reports **7**, 1 (2017).
- [46] S. A. Khrapak, Plasma Physics and Controlled Fusion **58**, 014022 (2015).